

# Magnetic Resonance Fingerprinting

- **Journal:** Nature
- **Authors:** Dan Ma, Vikas Gulani, Nicole Seiberlich, Kecheng Liu, Jeffrey L. Sunshine, Jeffrey L. Duerk, and Mark A. Griswold (2013)

# Contents

- Summary
- Introduction
- Generation and Recognition of MRF Signals
- Validation of the Concept
- Accelerated MRF Acquisitions
- Motion Error Tolerance in MRF
- Accuracy and efficiency of MRF
- Discussion and Conclusions
- Methods

# Summary

- MRF thus provides an alternative way to quantitatively detect and analyse complex changes that can represent physical alterations of a substance or early indicators of disease.
- When paired with an appropriate **pattern-recognition algorithm**, MRF inherently suppresses measurement errors and can thus improve measurement accuracy.

# Introduction

- Magnetic resonance acquisitions are often restricted to a qualitative or 'weighted' measurement.
- The magnetic resonance signal intensity is almost never quantitative by itself.
- The quantitative analysis of magnetic resonance results typically focuses on differences between spectral peaks, spatial locations or different points in time.
- Multiparametric measurements are almost always impractical owing to scan time limits and a high sensitivity to the measurement set-up and experimental conditions.

- MRF uses a pseudorandomized acquisition that causes the signals from different materials or tissues to have a unique signal evolution or **fingerprint** that is simultaneously a function of the multiple material properties under investigation.
- The processing after acquisition involves a pattern recognition algorithm to match the fingerprints to a predefined dictionary of predicted signal evolutions.
- MRF has the potential to quantitatively examine many magnetic resonance parameters simultaneously given enough scan time.
- MRF opens the door to computer-aided multiparametric magnetic resonance analyses, similar to genomic or proteomic analyses.

# Generation and Recognition of MRF Signals

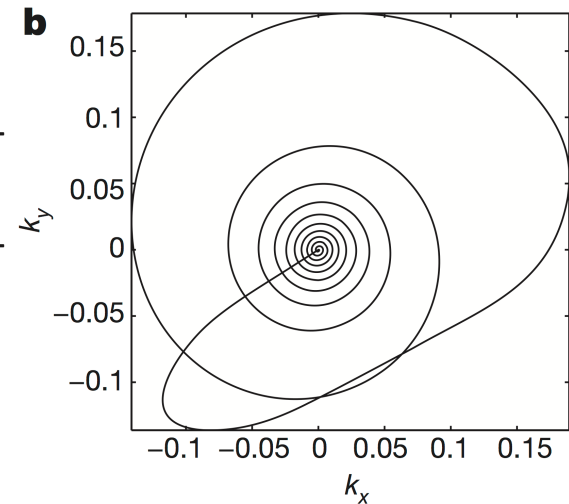
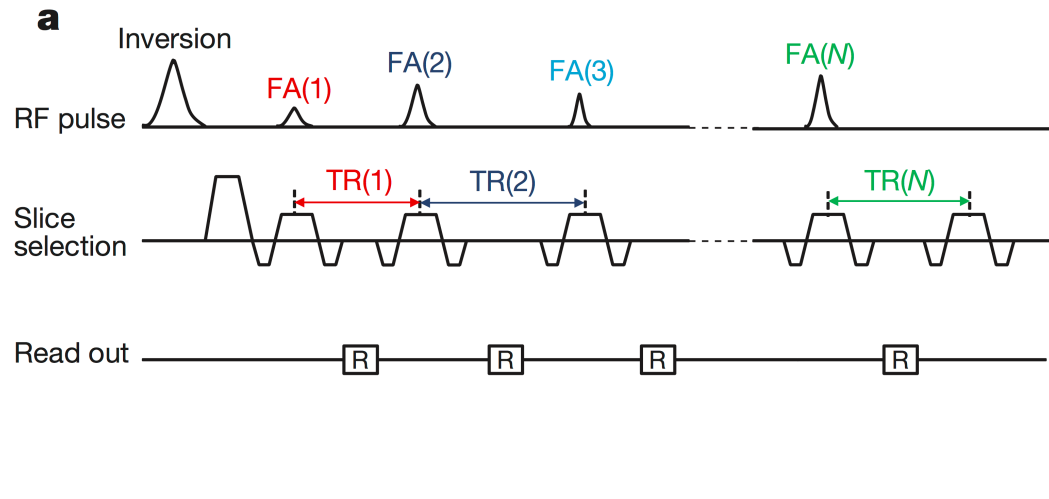
- Unique signal evolutions, or **fingerprints** is possible through continuous variation of the acquisition parameters throughout the data collection.
- Variations in the pulse sequence parameters have been used previously in MRI and magnetic resonance spectroscopy to reduce the signal oscillations and to improve the spectral response.
- MRF can be achieved by varying acquisition parameters, such as the flip angle and phase of radio frequency pulses, the repetition time, echo time and sampling patterns, in a pseudorandom manner.

- The separation of the signal into different material or tissue types can be achieved through **pattern recognition**.
- In the current implementation, we construct a dictionary that contains signal evolutions from all foreseeable combinations of materials and system-related parameters—for example, the longitudinal relaxation time,  $T_1$ , the transverse relaxation time,  $T_2$ , off-resonance frequency, diffusion and magnetization transfer are included in this study.
- Once this dictionary of possible signal evolutions is generated, a **matching or pattern recognition algorithm** is then used to select a signal vector or a weighted set of signal vectors from the dictionary that best correspond to the observed signal evolution.

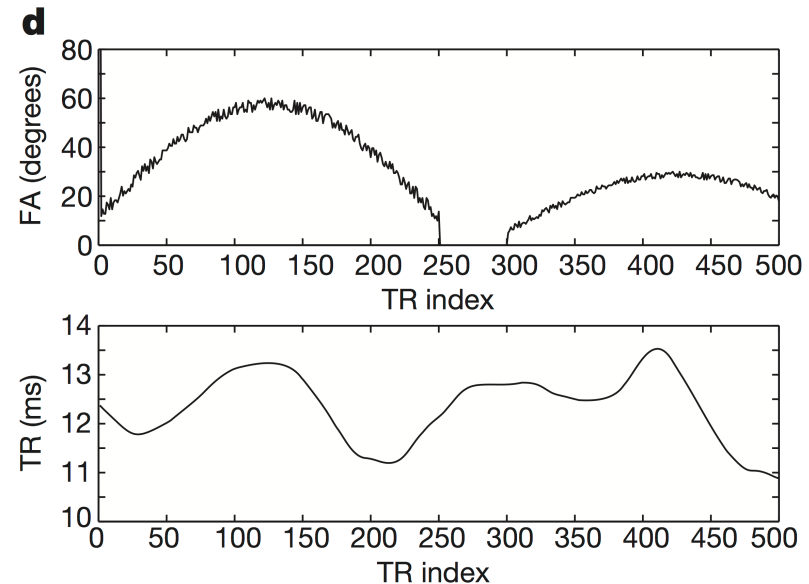
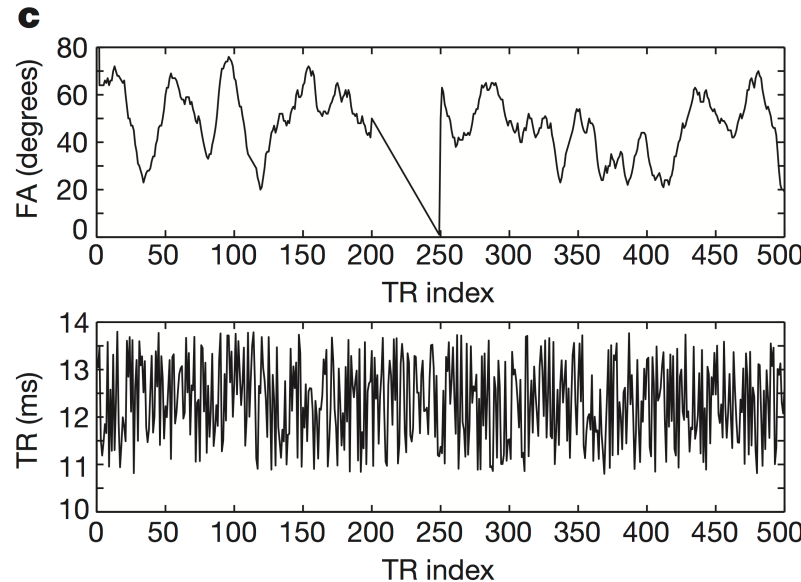
# Validation of the Concept

- **Inversion-recovery balanced steady state free-precession (IR-bSSFP)** sequence was used ([Fig. 1a](#)).
- After each radio-frequency pulse, one interleaf of a **variable density spiral (VDS)** read out was acquired, as shown in [Fig. 1b](#).
- Such a VDS trajectory has been used in fast imaging and for the reduction of undersampling errors.
- Two MRF acquisition patterns with randomized flip angle and repetition time were used as shown in [Fig. 1c and d](#).

- a, Acquisition sequence diagram.
- b, One variable density spiral trajectory was used per repetition time.

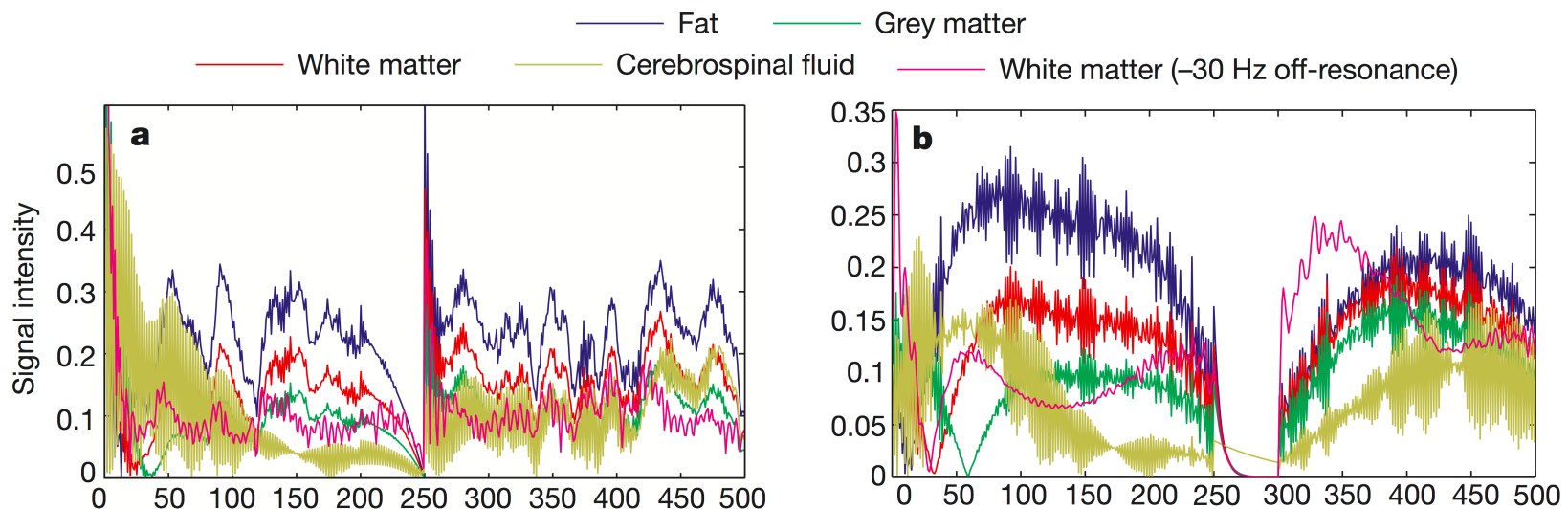


- c, d, Examples of the first 500 points of flip angle and repetition time patterns.

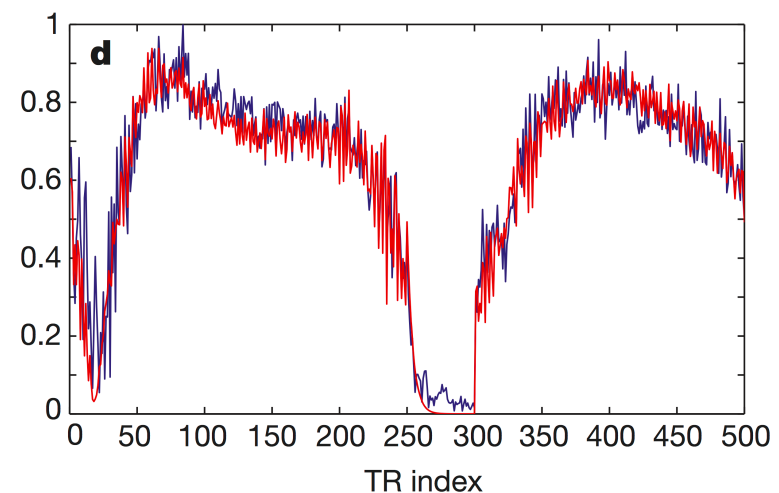
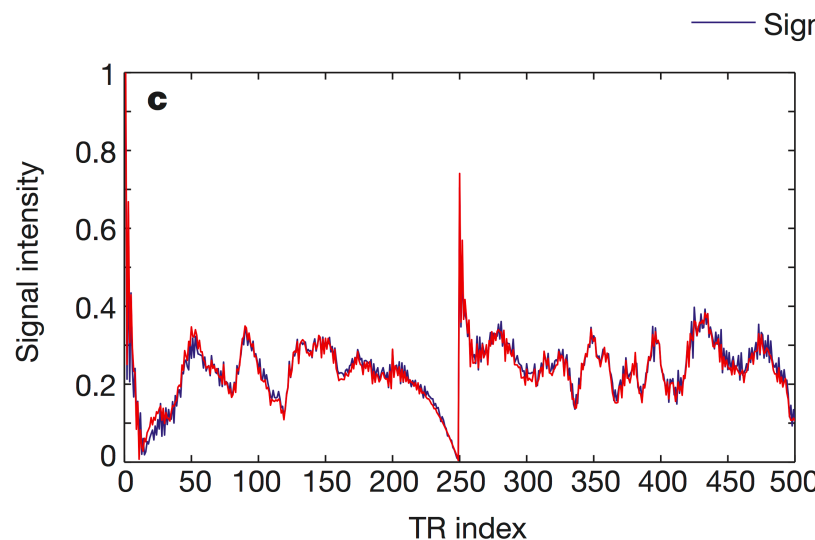


- Figure 2a and b show the simulated signal evolution curves that would be expected from four commonly encountered tissues of the brain.
- The signal levels in these evolutions represent a large fraction of the equilibrium magnetization.
- Figure 2c and d show an acquired signal evolution curve from fully sampled experiments on manufactured agar 'phantoms' and its match to the dictionary by using the acquisition pattern shown in Fig. 1c and d, along with the recovered  $T_1$ ,  $T_2$ , proton density ( $M_0$ ) and off-resonance frequency values.

- a, b, Simulated signal evolution curves corresponding to four normal brain tissues using the sequence patterns in Fig. 1c and d.



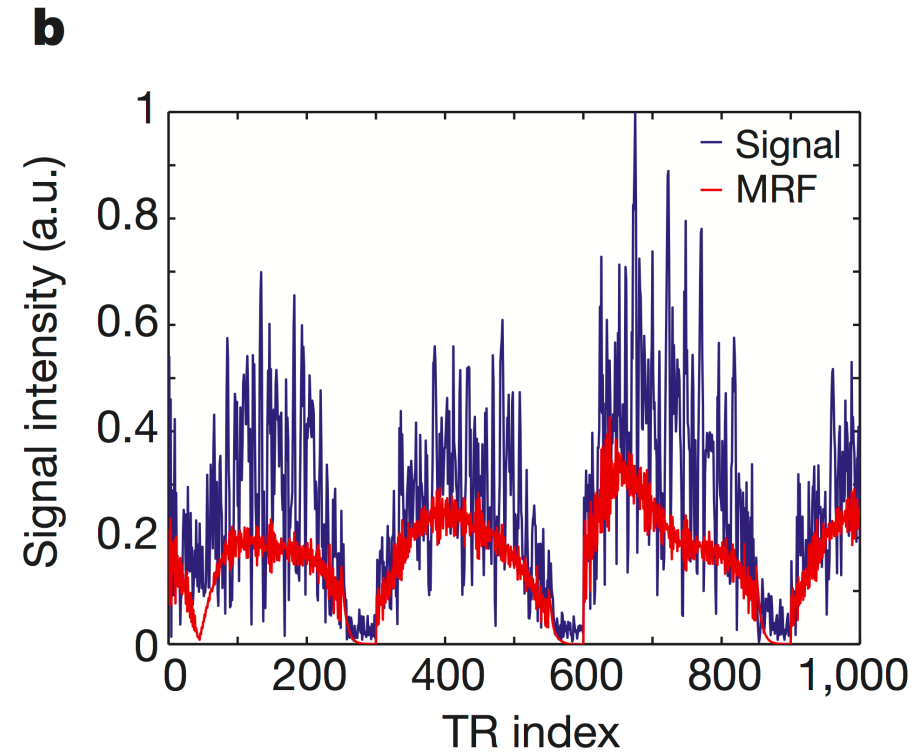
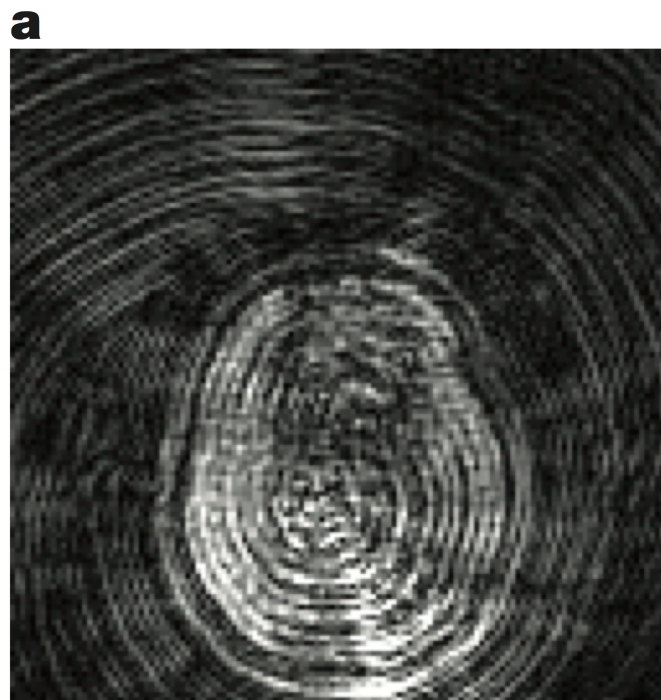
- c, d, Measured signal evolutions from one of eight phantoms using different sequence patterns and their dictionary match.



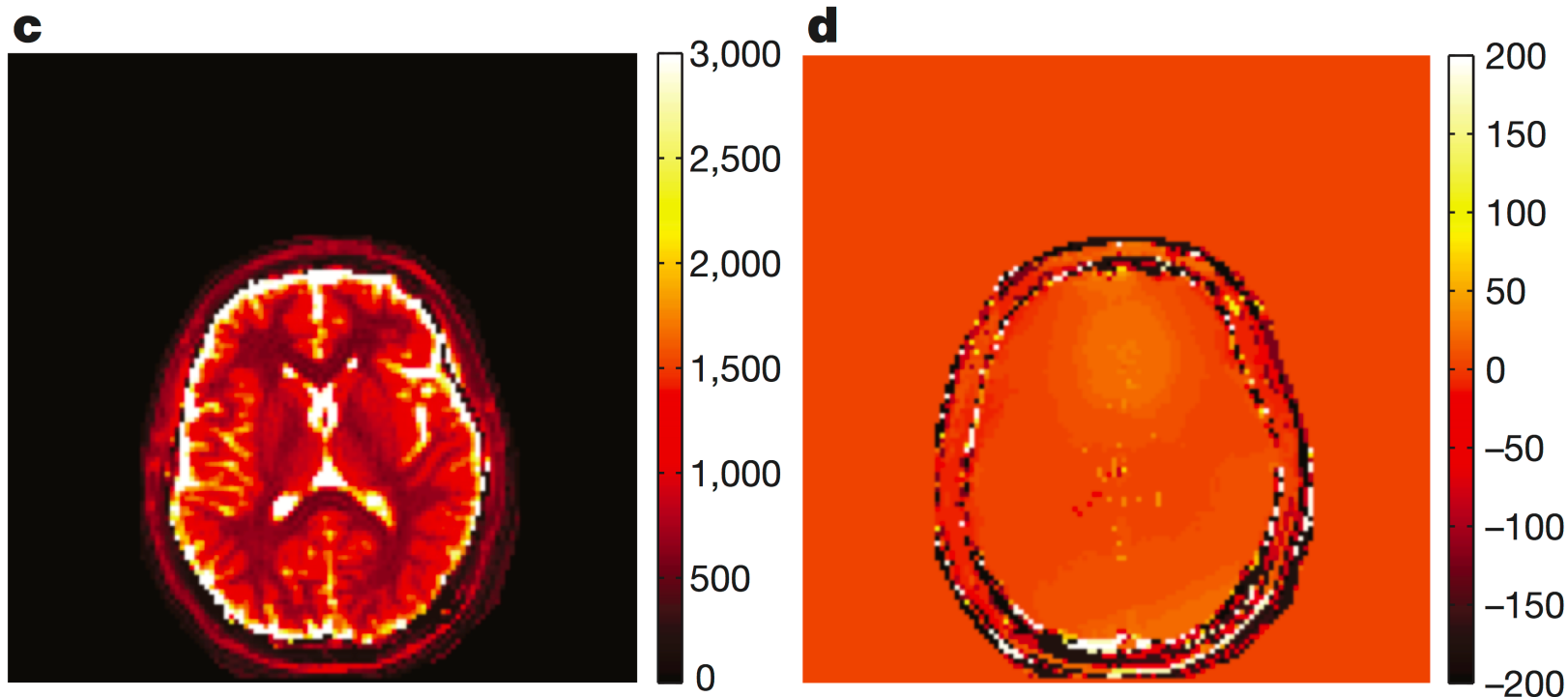
# Accelerated MRF Acquisitions

- Because MRF is based on pattern recognition in a setting where the form of all predicted signal evolutions is known, MRF should be less sensitive to errors during the measurement.
- The interaction of the temporal and spatial incoherence possible in MRF provides new opportunities to accelerate image acquisition through rejection of spatial undersampling errors.
- Figure 3c–f shows that high quality estimates of the magnetic resonance parameters are generated even with this significant level of undersampling.
- 220 Hz chemical shift of fat protons is clearly visualized in the off-resonance map.

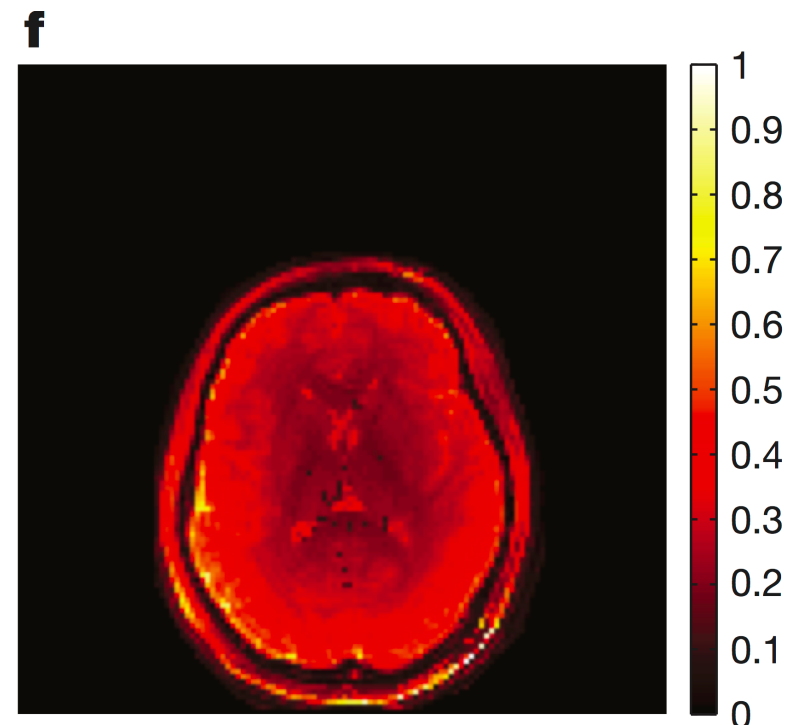
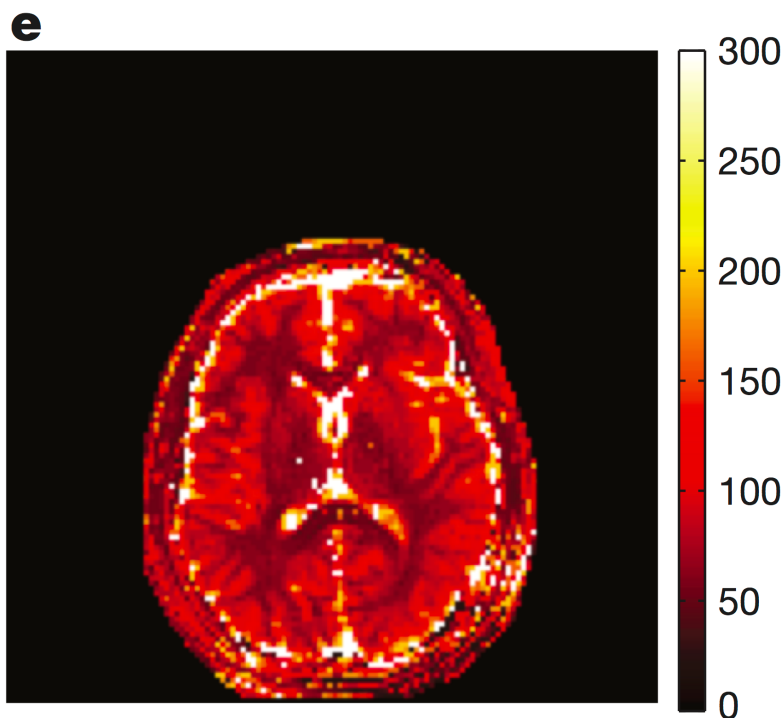
- a, An image was reconstructed from only one spiral readout, demonstrating the significant errors from undersampling.
- b, One example of acquired single evolution and its match to the dictionary.



- c,  $T_1$  (colour scale, milliseconds).
- d, off-resonance frequency (colour scale, hertz).



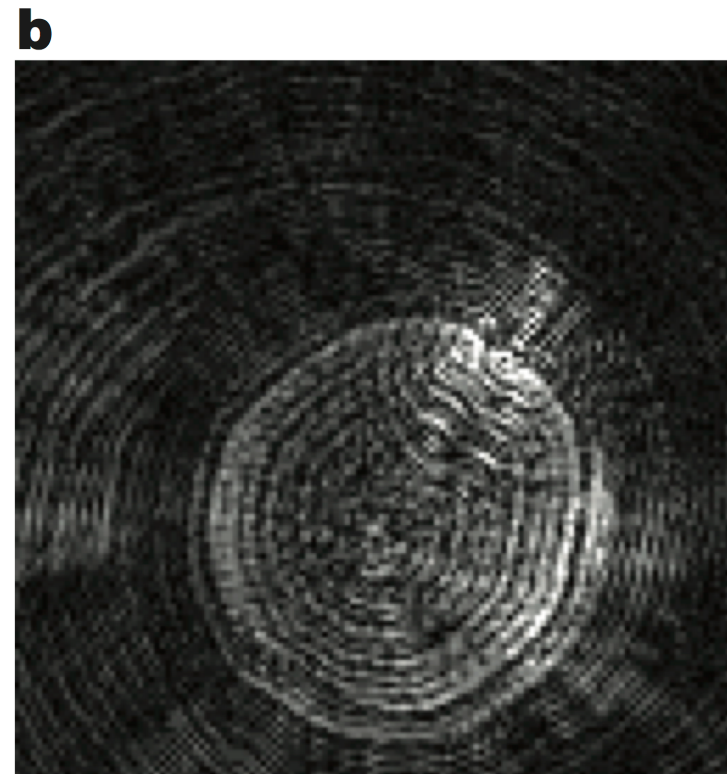
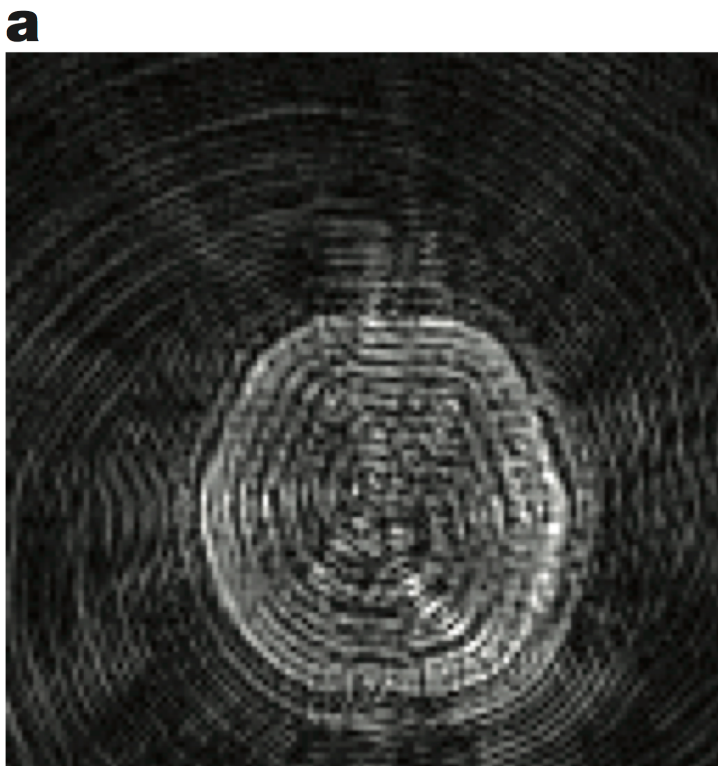
- e,  $T_2$  (colour scale, milliseconds).
- f, proton density ( $M_0$ ) (normalized colour scale).



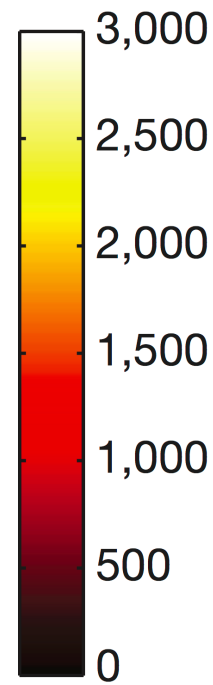
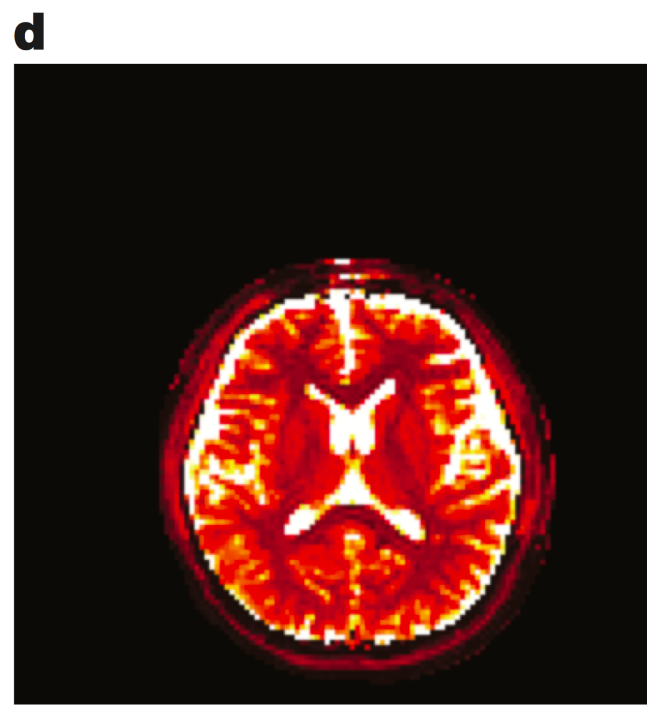
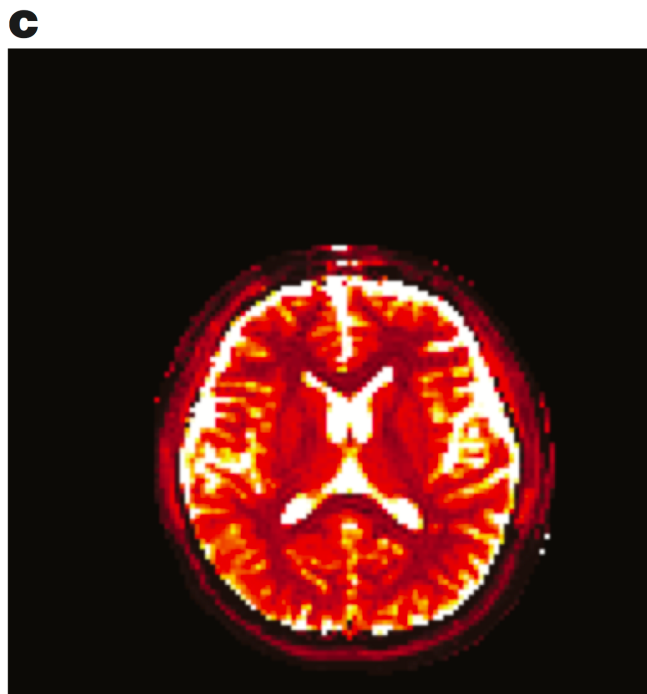
# Motion Error Tolerance in MRF

- The subject was instructed to randomly move his head for the last 3 s of a total 15-s scan.
- The maps acquired during motion show almost no sensitivity to the motion, and show nearly the same quality and anatomy as the maps from the motion-free data.
- The signal changes resulting from motion were uncorrelated with the evolutions included in the dictionary, and were largely ignored by the pattern recognition algorithm.

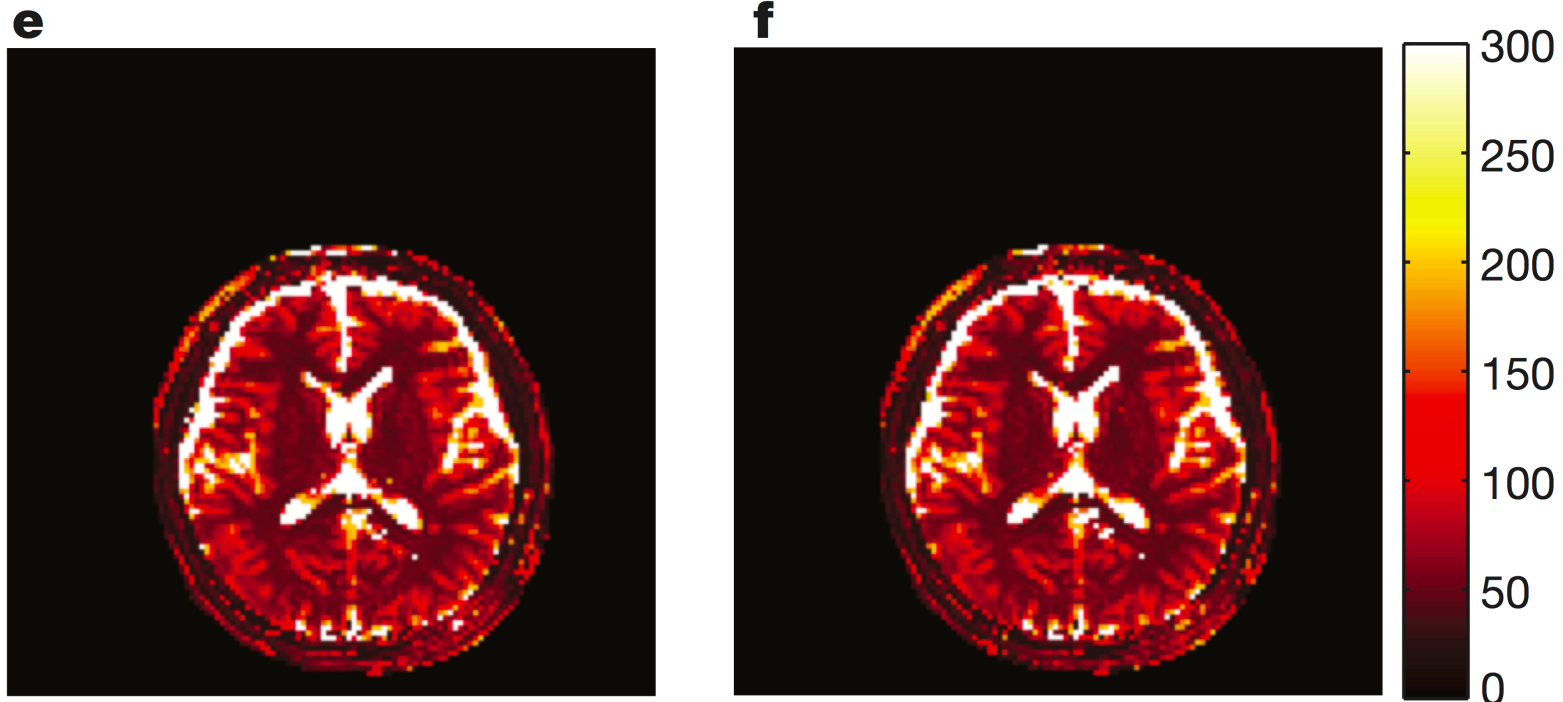
- a, b, Reconstructed images demonstrate the large shift in the head position.



- c, no motion.
- d, from entire 15 s that includes the motion.



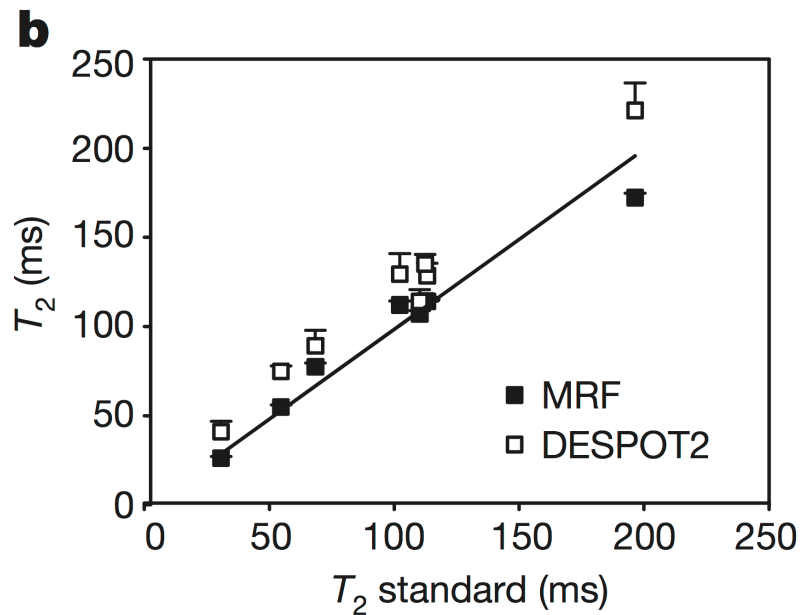
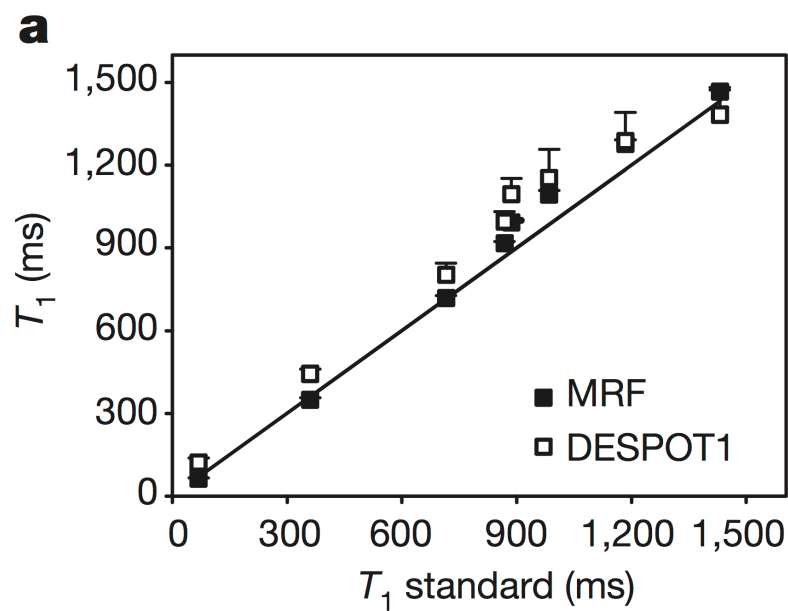
- e, no motion.
- f, from entire 15 s that includes the motion.



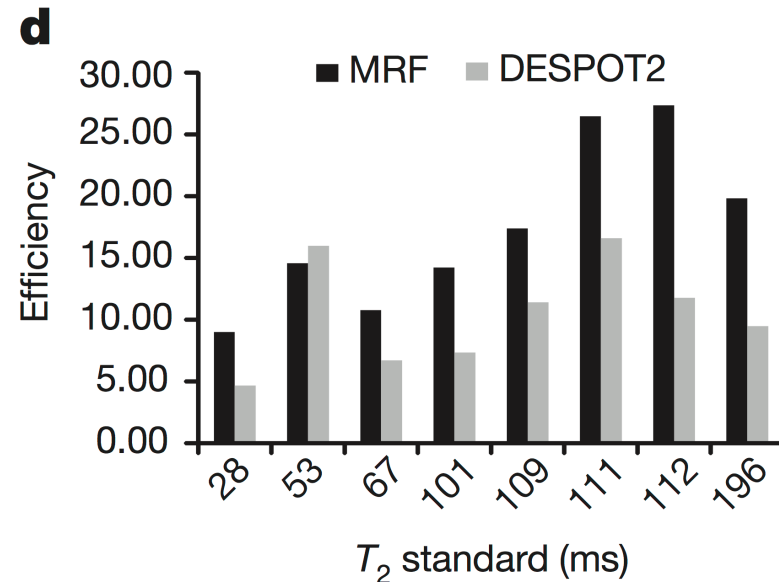
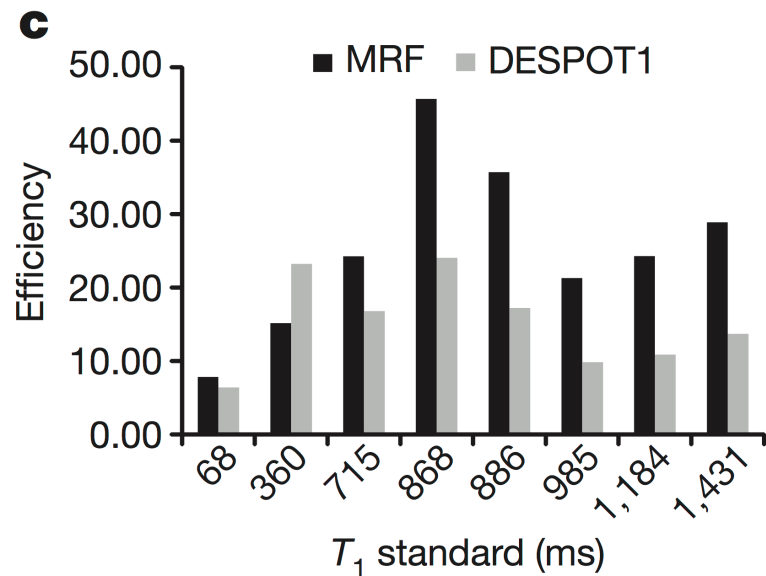
# Accuracy and Efficiency of MRF

- The accuracy and efficiency of the MRF acquisitions were compared with DESPOT1 and DESPOT2 (driven equilibrium single pulse observation of  $T_1$  and  $T_2$ , respectively).
- Figure 5a and b compares the phantom  $T_1$  and  $T_2$  values from these methods.
- The high concordance correlation coefficients indicate that both methods are in good agreement with standard spin-echo measurements.
- As can be seen in Fig. 5c and d, MRF outperforms both DESPOT1 and DESPOT2 by an average factor of 1.87 and 1.85, respectively.
- Because there is no steady state in the signal evolution from MRF, new information will be continuously added by longer acquisitions.

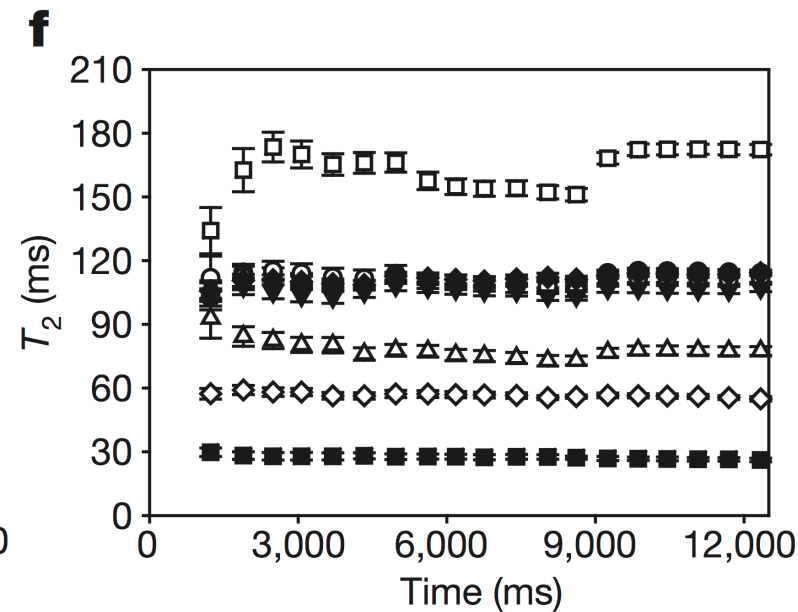
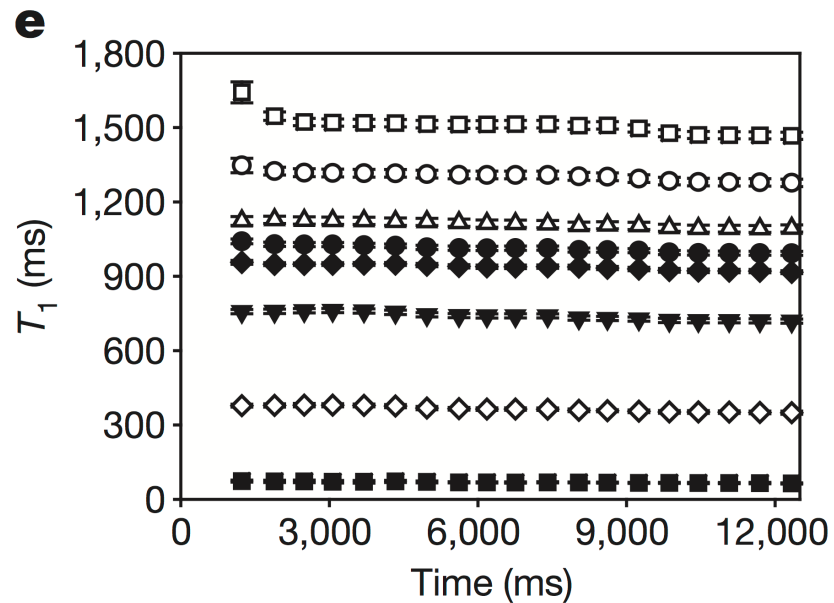
- a, b, The  $T_1$  and  $T_2$  values retrieved from MRF from eight phantoms are compared with those acquired from DESPOT1 (a), DESPOT2 (b) and a standard spin-echo sequence.



- c, d, The efficiency of MRF compared to DESPOT1 (c) and DESPOT2 (d).



- e, f, Obtained values of  $T_1$  (e) and  $T_2$  (f) as a function of acquisition time.



# Discussion and Conclusions

- Because there is no a **priori** requirement on the shape of the signal evolution curves, there are more degrees of freedom in designing an MRF acquisition.
- MRF has the potential to significantly reduce the effects of errors during acquisition through its basis in pattern recognition.
- Both MRF and DESPOT2 are based on a bSSFP sequence, which is known to be sensitive to field inhomogeneities.
- MRF could lead to the direct identification of a material, tissue or pathology solely on the basis of its fingerprint.
- Both the sequence design/implementation and post-processing methods will continue to be a significant open area of research.

# Methods

- Sequence Design
- Dictionary Design
- Data Acquisition
- Statistical Analysis

# Sequence Design

- The first sequence pattern shown in [Fig. 1c](#) used a **pseudorandomized series (Perlin noise)** of flip angle and a random repetition time between 10.5 ms and 14 ms.
- The second flip angle pattern in [Fig. 1d](#) used a series of repeating sinusoidal curves with a period of 250 repetition times and alternating maximum flip angles.
- A 600 ms delay was added between each of the periods to allow for both differential magnetization recovery according to  $T_1$  and differential signal decay according to  $T_2$ .
- The variable density spiral-out trajectory was designed to have 5.8 ms readout time in each repetition time and to have zero and first moment gradient compensation using **minimum-time gradient design**.

# Dictionary Design

- The ranges of  $T_1$  and  $T_2$  for the in vivo study were chosen according to the typical physiological limits of tissues in the brain.
- Since magnetic resonance is sensitive to parts per million (p.p.m.) level deviations in the  $B_0$  field, different off-resonance frequencies were simulated for each combination of  $T_1$  and  $T_2$  parameters to incorporate the effects of signal evolutions in different  $B_0$  fields.
- One dictionary entry was selected for each measured pixel location using template matching.
- The dictionary entry with the highest dot-product was then selected as most likely to represent the true signal evolution.

# Data Acquisition

- Images from each acquisition block were reconstructed separately using **non-uniform Fourier transform (NUFFT)**.
- $T_1$  values were calculated pixel-wise using a standard three-parameter nonlinear least squares fitting routine to solve the equation:

$$S(\text{TR}) = a + b e^{\text{TR}} / T_1$$

- $T_2$  values were determined in a pixel-wise fashion using a two-parameter nonlinear least squares fitting routine to solve the equation:

$$S(\text{TE}) = a e^{-\text{TE}} / T_2$$

# Statistical Analysis

- Quantitative estimates of the errors and efficiencies were calculated pixel-wise using a **bootstrapped Monte Carlo method**.
- Two sets of raw data were acquired for each sequence: the encoded signal and a separate acquisition that only contained noise.
- 50 reconstructions were then calculated by randomly resampling the acquired noise and adding it to the raw data before reconstruction and quantification.
- The **concordance correlation coefficients ( $\rho_c$ )** were calculated using the equation:

$$\rho_c = \frac{2S_{12}}{S_1^2 + S_2^2 + (\bar{Y}_2 - \bar{Y}_1)^2}$$

- The efficiency of the methods was calculated using  $T_n NR / \sqrt{T_{\text{seq}}}$